Recirculation time and liquid slug mass transfer in co-current upward and downward Taylor flow

Semih Kececi[a,b], Martin Wörner[b], Alexandru Onea[c], Hakan Serhad Soyhan[a]

[a] Department of Mechanical Engineering, University of Sakarya, 54187 Sakarya, Turkey

[b] Forschungszentrum Karlsruhe, Institut für Kern- und Energietechnik, Postfach 3640, 76021 Karlsruhe, Germany

[c] Forschungszentrum Karlsruhe, Institut für Neutronenphysik und Reaktortechnik, Postfach 3640, 76021 Karlsruhe, Germany

Abstract

In this paper we investigate the recirculation time (τ) in the liquid slug of laminar Taylor flow theoretically and numerically. Theoretically, we develop a correlation for τ in rectangular channels, which depends on the aspect ratio and the ratio (ψ) between the bubble velocity and the total superficial velocity. This correlation suggests that τ is - for a given value of ψ - larger in upward than in downward Taylor flow because of buoyancy. The evaluation of τ from direct numerical simulations of Taylor flow confirms this result. The lower value of τ suggests that the sequential mass transfer between the gas bubble, the liquid slug and the channel wall is more efficient in downward than in upward flow. Numerical investigations of the overall wall-to-bulk mass transfer, which also contains the contribution through the liquid film between the bubble and the channel wall, show, however, that upward Taylor flow is slightly more efficient than downward Taylor flow. This indicates that for heterogeneously catalyzed gas-liquid reactions in monolith reactors a general statement whether mass transfer in upward or downward Taylor flow is more efficient is not reasonable, since the overall mass transfer depends on a large number of hydrodynamic and physical-chemical parameters.

Keywords: recirculation time, Taylor flow, mass transfer, multiphase monolith reactors

1. Introduction

Bubble train flow or Taylor flow constitutes an attractive flow pattern for catalytic multiphase

monolith reactors [1],[2] because of its excellent mass transfer properties. It consists of a sequence of bubbles that almost fill the cross-section of a narrow channel and are separated by liquid slugs. Recent reaction studies [3], [4] have shown that Taylor flow is superior as compared to other two-phase flow patterns.

For heterogeneously catalyzed chemical reactions in Taylor flow, the mass transfer of chemical species from the gas bubble to the solid wall takes place by two parallel paths. Each path consists of two steps in series. The first path is given by the mass transfer from the lateral sides of the bubble into the liquid film surrounding the bubble body (step 1), and by the mass transfer from the liquid film toward the solid wall (step 2). The second path consists of the mass transfer from the front and rear cap of the bubble to the liquid slug (step 1) and from the liquid slug toward the solid wall (step 2). The mass transfer of this second path is strongly affected by the recirculation in the liquid slug. The intensity of this recirculation can be quantified by the time needed for the liquid to move from one end of the slug to the other end, T_L . A second characteristic time scale is the time needed by the liquid slug to travel a distance of its own length. This time is given by $T_S \equiv L_S / U_B$, where L_S is the length of the liquid slug and U_B is the bubble velocity. Thulasidas et al. [5] defined the ratio of both times as the non-dimensional recirculation time

$$\tau \equiv \frac{T_L}{T_S} = \frac{T_L U_B}{L_S} \tag{1}$$

Multiphase monolith reactors can be operated in co-current upward or co-current downward flow. Recent experimental investigations of Taylor flow in a square mini-channel suggest that mass transfer between the slug and the channel wall may be more efficient in upward than in downward flow [6]. This is attributed to the lower recirculation time.

In this paper we perform, to our knowledge for the first time, a theoretical analysis of the recirculation time in laminar Taylor flow in rectangular channels. Based on this analysis we develop in section 2 a predictive correlation which indicates that the recirculation time in Taylor flow is larger in upward than in downward flow because of buoyancy. In section 3 we confirm this result for a square channel by evaluations of the recirculation time from direct numerical simulation (DNS)

results. In this section, we also discuss results of new numerical investigations on the wall-to-bulk mass transfer in co-current upward and downward Taylor flow at similar values of the total superficial velocity. In section 4 we present the conclusions.

2. Theoretical analysis of recirculation time in Taylor flow

The evaluation of the time T_{L} requires the knowledge of the velocity field within the liquid slug. Here, we assume that the liquid slug is sufficiently long to form a fully developed Poiseuille profile. According to Thulasidas et al. [5] this assumption is valid when the liquid slug length is larger than about 1.5 times the hydraulic diameter of the channel, D_{h}. Neglecting end effects in the liquid slug close to the front of the trailing and the rear of the leading bubble, we introduce the approximation

$$T_{\mathrm{L}} = \frac{L_{\mathrm{S}}}{\langle V_{\mathrm{Po}} \rangle_{A_0}} \tag{2}$$

Here,

$$\langle V_{\mathrm{Po}} \rangle_{A_0} = \frac{\iint_{A_0} V_{\mathrm{Po}} \mathrm{d}A}{\iint_{A_0} \mathrm{d}A} = \frac{1}{A_0} \iint_{A_0} V_{\mathrm{Po}} \mathrm{d}A \tag{3}$$

is the mean velocity in the channel cross section area A_0, where the Poiseuille velocity profile in the moving frame of reference, V_{Po}, is positive. Then, the non-dimensional recirculation time is given by

$$\tau \equiv \frac{T_{\mathrm{L}}}{T_{\mathrm{S}}} = \frac{U_{\mathrm{B}}}{\langle V_{\mathrm{Po}} \rangle_{A_0}} = \frac{\iint_{A_0} \mathrm{d}A}{\iint_{A_0} (V_{\mathrm{Po}}/U_{\mathrm{B}}) \mathrm{d}A} \tag{4}$$

2.1. Circular channel

In a circular channel with radius R, the Poiseuille velocity profile in the frame of reference moving with the bubble is given by

$$V_{\mathrm{Po}}^{\mathrm{cir}}(r) = U_{\mathrm{L,max}}^{\mathrm{cir}} \left(1 - \frac{r^2}{R^2}\right) - U_{\mathrm{B}} = C_{\mathrm{Po}}^{\mathrm{cir}} U_{\mathrm{L,mean}}^{\mathrm{cir}} \left(1 - \frac{r^2}{R^2}\right) - U_{\mathrm{B}} \tag{5}$$

where $C_{\mathrm{Po}}^{\mathrm{cir}} = U_{\mathrm{L,max}}^{\mathrm{cir}} / U_{\mathrm{L,mean}}^{\mathrm{cir}} = 2$. In an incompressible Taylor flow, the mean velocity in the liquid slug is equal to the total superficial velocity J, so that $U_{\mathrm{L,mean}} = J$. A recirculation pattern in the liquid slug occurs for $U_{\mathrm{B}} < U_{\mathrm{L,max}}$ or $\psi \equiv U_{\mathrm{B}} / J < C_{\mathrm{Po}}$, i.e. in a circular channel for $\psi < 2$. From Eq.

(5) one obtains for the radial position r_0, where the velocity $V_{\mathrm{Po}}^{\mathrm{cir}}$ is zero, the result

$$\frac{r_0}{R} = \sqrt{1-\frac{\psi}{2}} \tag{6}$$

With $A_0 = \pi r_0^2$ and $\mathrm{d}A = 2\pi r \mathrm{d}r$ Thulasidas et al. [5] obtained from Eq. (4) the relation

$$\tau_{\mathrm{cir}} = \frac{U_{\mathrm{B}} r_0^2}{2\int_0^{r_0} V_{\mathrm{Po}}^{\mathrm{cir}}(r) r \mathrm{d}r} \tag{7}$$

Introducing Eq. (5) and Eq. (6) in Eq. (7) and performing the integration yields

$$\tau_{\mathrm{cir}}(\psi) = \left(\frac{1}{\psi} - \frac{1}{2}\right)^{-1} = \frac{C_{\mathrm{Po}}^{\mathrm{cir}}}{\phi^{-1} - 1} \tag{8}$$

where $\phi \equiv C_{\mathrm{Po}}^{\mathrm{cir}} / \psi$. The velocity ratio ψ is in the range $1 \le \psi < 2$ so that the minimal recirculation time in a circular channel is 2 while it becomes infinity for $\psi \to 2$. From Eq. (6) we obtain for the non-dimensional area where $V_{\mathrm{Po}}^{\mathrm{cir}} \ge U_{\mathrm{B}}$ the result

$$\frac{A_0}{A_{\mathrm{ch}}} = \frac{\pi r_0^2}{\pi R^2} = \frac{2-\psi}{2} \tag{9}$$

In Taylor flow, the cross-sectional regions with bypass flow (close to the walls) and recirculation flow (in the channel center) are separated by the "dividing streamline" [5]. The position of the dividing streamline is obtained from the condition that the total axial flow rate within the recirculation area is zero in the moving frame of reference. For a circular channel this requirement is equivalent to the condition

$$2\pi \int_{r_1}^{R} V(r) r \mathrm{d}r = \pi R^2 (U_{\mathrm{B}} - J) \tag{10}$$

given in [5] which yields

$$\frac{r_1}{R} = \sqrt{2-\psi} \tag{11}$$

Thus, in a circular channel the non-dimensional cross-sectional recirculation area is $A_1 / A_{\mathrm{ch}} = 2 - \psi$ and it is $A_1 / A_0 = 2$ for any value of ψ.

2.2. Rectangular channel

We consider a rectangular channel with dimensions $2a$ and $2b$ as displayed in Fig. 1. The cross-

sectional area of the channel is $A_{\mathrm{ch}} = 4ab$ and its aspect ratio is $\alpha \equiv b/a \le 1$. The origin of the coordinate system is located in the channel center so that $-a \le z \le a$ and $-b \le y \le b$. In the moving frame of reference, the laminar Poiseuille velocity profile for this channel is given by [7]

$$V_{\mathrm{Po}}^{\mathrm{rec}}(y,z) = \frac{64}{\pi^3} J \frac{\displaystyle\sum_{n=1,3,5}^{\infty} \frac{(-1)^{\frac{n-1}{2}}}{n^3}\left[1-\frac{\cosh\left(\frac{n\pi}{2a}y\right)}{\cosh\left(\frac{n\pi b}{2a}\right)}\right]\cos\left(\frac{n\pi}{2a}z\right)}{1-\dfrac{192a}{\pi^5 b}\displaystyle\sum_{n=1,3,5}^{\infty}\frac{1}{n^5}\tanh\left(\frac{n\pi b}{2a}\right)} - U_{\mathrm{B}} \tag{12}$$

Since for this velocity profile an analytical evaluation of the recirculation time according to Eq. (4) is not practicable, we adopt the approximation

$$V_{\mathrm{Po}}^{\mathrm{rec}}(Y,Z) = C_{\mathrm{Po}}^{\mathrm{rec}} J (1-Y^n)(1-Z^m) - U_{\mathrm{B}} \tag{13}$$

first proposed by Purday [8]. Here, it is $Y \equiv y/b$, $Z \equiv z/a$ and

$$C_{\mathrm{Po}}^{\mathrm{rec}} = \frac{U_{\mathrm{L,max}}^{\mathrm{rec}}}{U_{\mathrm{L,mean}}^{\mathrm{rec}}} = \frac{m+1}{m}\frac{n+1}{n} \tag{14}$$

The values of n and m depend on the aspect ratio. Here, we adopt the following correlations proposed by Natarajan and Lakshmanan [9]

$$n = \begin{cases} 2 & \text{for} \quad 0 \le \alpha \le 1/3 \\ 2 + 0.3(\alpha - 1/3) & \text{for} \quad 1/3 \le \alpha \le 1 \end{cases} \tag{15}$$

$$m = 1.7 + 0.5\alpha^{-1.4} \tag{16}$$

For this velocity profile, a Taylor flow with recirculation pattern in the liquid slug occurs for $1 \le \psi < C_{\mathrm{Po}}^{\mathrm{rec}}$ or $1/C_{\mathrm{Po}}^{\mathrm{rec}} \le \phi < 1$, respectively.

In the sequel, we will utilize the curves $Z_\lambda = Z(Y, C_{\mathrm{Po}}^{\mathrm{rec}}, \lambda)$ where the ratio $\lambda \equiv V_{\mathrm{Po}}^{\mathrm{rec}}/U_{\mathrm{B}}$ is constant. Here, λ is in the range $-1 \le \lambda \le C_{\mathrm{Po}}^{\mathrm{rec}}/\psi - 1 = \phi^{-1} - 1$. From Eq. (13) we obtain

$$Z_\lambda = \left(1 - \frac{\psi}{C_{\mathrm{Po}}^{\mathrm{rec}}}\frac{1+\lambda}{1-Y^n}\right)^{\frac{1}{m}} = \left(\frac{Y_{\mathrm{max},\lambda}^n - Y^n}{1-Y^n}\right)^{\frac{1}{m}} \tag{17}$$

Here,

$$Y_{\mathrm{max},\lambda} \equiv \left[1-(1+\lambda)\phi\right]^{\frac{1}{n}} \tag{18}$$

is the value of Y for $Z = 0$. For the cross-sectional area where $V_{\mathrm{Po}}^{\mathrm{rec}}/U_{\mathrm{B}} \ge \lambda$ we obtain the result

$$\iint_{A_\lambda} \mathrm{d}A = 4ab \int_0^{Y_{\max,\lambda}} \int_0^{Z_\lambda(Y)} \mathrm{d}Z\mathrm{d}Y = 4ab \int_0^{Y_{\max,\lambda}} Z_\lambda(Y)\mathrm{d}Y = 4abY_{\max,\lambda} \int_0^1 \left(\frac{1-u^n}{Y_{\max,\lambda}^{-n} - u^n} \right)^{\frac{1}{m}} \mathrm{d}u \tag{19}$$

Here, we used the substitution $u \equiv Y / Y_{\max,\lambda}$. A similar but lengthy evaluation yields

$$\begin{aligned} \iint_{A_\lambda} \frac{V}{U_\mathrm{B}} \mathrm{d}A &= 4ab \int_0^{Y_{\max,\lambda}} \int_0^{Z_\lambda} \left[\frac{1}{\phi}(1-Y^n)(1-Z^m) - 1 \right] \mathrm{d}Z\mathrm{d}Y \\ &= \frac{4abY_{\max,\lambda}}{1-Y_{\max,\lambda}^n} \int_0^1 \left(\frac{1-u^n}{Y_{\max,\lambda}^{-n} - u^n} \right)^{\frac{1}{m}} \left(\lambda(1-Y_{\max,\lambda}^n u^n) + \frac{m-\lambda}{m+1} Y_{\max,\lambda}^n (1-u^n) \right) \mathrm{d}u \end{aligned} \tag{20}$$

Setting $\lambda = 0$, we obtain from Eqs. (19), (20) and (4) the results

$$\frac{A_0}{A_\mathrm{ch}} = (1-\phi)^{\frac{1}{n}} \int_0^1 \left(\frac{1-u^n}{(1-\phi)^{-1} - u^n} \right)^{\frac{1}{m}} \mathrm{d}u \tag{21}$$

$$\tau_\mathrm{rec} = \frac{1}{\phi^{-1}-1} \frac{m+1}{m} \frac{\displaystyle\int_0^1 \left(\frac{1-u^n}{(1-\phi)^{-1} - u^n} \right)^{\frac{1}{m}} \mathrm{d}u}{\displaystyle\int_0^1 \left(\frac{(1-u^n)^{m+1}}{(1-\phi)^{-1} - u^n} \right)^{\frac{1}{m}} \mathrm{d}u} \equiv \frac{K(\phi,n,m)}{\phi^{-1}-1} \tag{22}$$

Comparing the result for τ in a circular channel, Eq. (8), with that for a rectangular channel, Eq. (22), shows a similar functional dependence of τ on ϕ. Both expressions differ only by the numerator which is constant for the circular channel and is a function of α and ϕ for the rectangular channel.

As mentioned above, the position of the dividing streamline is determined by the condition that the net flow rate in the recirculation area A_1 vanishes. Setting Eq. (20) to zero yields

$$\lambda_1 = \frac{\lambda_1 - m}{m+1} Y_{\max,\lambda_1}^n \frac{\displaystyle\int_0^1 \left(\frac{(1-u^n)^{1+m}}{1/Y_{\max,\lambda_1}^n - u^n} \right)^{\frac{1}{m}} \mathrm{d}u}{\displaystyle\int_0^1 \left(\frac{1-u^n}{1/Y_{\max,\lambda_1}^n - u^n} \right)^{\frac{1}{m}} (1-Y_{\max,\lambda_1}^n u^n) \mathrm{d}u} \tag{23}$$

where $Y_{\max,\lambda_1}^n = 1-(1+\lambda_1)\phi$. This equation must be solved iteratively to determine $\lambda_1 = \lambda_1(\alpha,\phi)$. The values of λ_1 are then used to compute $A_1 = A_1(\alpha,\phi)$ from Eq. (19).

The present analysis shows that τ, A_0 / A_ch and A_1 / A_ch are functions of $\phi = \psi / C_\mathrm{Po}^\mathrm{rec} = U_\mathrm{B} / U_\mathrm{L,max}$ and the channel aspect ratio α. The latter determines the values of n and

m via Eqs. (15) and (16), and $C_{\mathrm{Po}}^{\mathrm{rec}}$ via Eq. (14). In the following we discuss the dependence of τ, A_0 / A_{ch}, and A_1 / A_{ch} on ψ for six different values of α, namely $\alpha = 1$, 0.5, 1/3, 0.25, 0.2 and 0.1. The integrals in Eqs. (19) – (23) are evaluated numerically using the numerical computing environment MATLAB. The results for τ as function of ψ are displayed in Fig. 2 and show a family of similar but shifted curves for the different values of α. For a certain value of ψ the recirculation time in a square channel is always smaller than in a circular channel. While the minimum value of τ is 2 in a circular channel, it is 1.757 in a square channel. Fig. 2 shows that for a rectangular channel with aspect ratio $\alpha = 0.5$ the relationship between τ and ψ is very similar to that in a circular channel. However, there is a cross-over of both curves for $\psi \approx 1.75$. As the aspect ratio decreases further, the recirculation time increases for a given value of ψ.

In Fig. 3 we display the results for $K = K(\alpha, \psi)$, defined by Eq. (22), for the six different aspect ratios considered. For a certain value of α the value of K depends only weakly on $\psi = \phi C_{\mathrm{Po}}^{\mathrm{rec}}$ and decreases slightly as ψ increases. There is, however, a notable dependence of K on α and K decreases as α decreases. To avoid the laborious numerical integrations necessary to determine K for general values of α and ψ, we approximate K by the relation

$$K(\alpha, \psi) = A(\alpha) + (1 - \psi) B(\alpha) \tag{24}$$

which is linear in ψ. By considering 13 distinct aspect ratios in the range $0.1 \le \alpha \le 1$ we found that K is well fitted by Eq. (24) for $A(\alpha) = 2 - 0.56 \exp(-\alpha / 0.364)$ and $B(\alpha) = 0.0475 - 0.0533 \exp(-\alpha / 0.285)$. This correlation is shown in Fig. 3 by symbol "+".

In Fig. 4 we compare the results for A_0 / A_{ch} and A_1 / A_{ch} as function of ψ for different values of α with the respective non-dimensional areas for a circular channel. The values of $\lambda_1 = \lambda_1(\alpha, \psi)$ used to determine A_1 are displayed in the inset graphics of Fig. 3. The main difference between a rectangular and a circular channel is that in a rectangular channel the area A_1 / A_{ch} does not approach unity for small values of ψ but only a value of about 0.75 regardless of the value of α. This

behavior can be attributed to the low liquid velocities in the corners of the rectangular channel.

The utilization of the analytical relations obtained in this section for τ, A_0 / A_{ch} and A_1 / A_{ch} for practical purposes requires knowledge of $\psi = U_B / J$. This ratio depends on the capillary number $Ca \equiv \mu_L U_B / \sigma$. Here, μ_L is the liquid viscosity and σ the coefficient of surface tension. In addition, ψ may depend on the bubble size and channel orientation. The corresponding functional relationships for ψ must be obtained from experiments or from direct numerical simulations. This topic will be considered in Section 3. When ψ is known, then the dimensional recirculation time defined as the time for the liquid to move from one end of the slug to the other end can be estimated as

$$T_L = \frac{L_S \tau}{U_B} = \frac{L_S}{U_B} \frac{K(\alpha,\psi)}{C_{Po}/\psi - 1} = \frac{L_S}{J} \frac{K(\alpha,\psi)}{C_{Po} - \psi} \tag{25}$$

For a circular channel it is $K = C_{Po}^{cir} = 2$. For a rectangular channel K is given by Eq. (24) and C_{Po}^{rec} by Eq. (14).

We note that the above analysis is purely kinematic in nature, as it relies only on the ratio $\phi = \psi / C_{Po}^{rec} = U_B / U_{L,max}$. While the bubble size and shape are not considered at all, it is evident that both will influence U_B and J and therefore will determine the values of ϕ and ψ, respectively.

3. Numerical investigations for Taylor flow in a square channel

In this section we utilize results of three-dimensional direct numerical simulations for laminar bubble train flow and Taylor flow to evaluate and analyze the recirculation time in a square channel. The numerical simulations have been performed by our in-house computer code TURBIT-VOF. The code solves the single-field Navier-Stokes equation with surface tension term for two immiscible Newtonian fluids with constant density, viscosity and surface tension. The dynamic evolution of the interface is described by a volume-of-fluid method with piecewise planar interface reconstruction. For details on the governing equations and numerical method we refer to [10].

In the sequel we consider simulation results for two different cases. In the first case, the channel cross section is 1 mm × 1 mm and the liquid phase is squalane [11]. In the second case the channel

cross-section is 2 mm × 2 mm, the liquid phase is silicon oil and the flow is co-current upward [10], [12],[13]. For comparison we perform in the present study one additional simulation for case 2 with the same fluid properties as case C in [13] but for co-current downward flow. In Table 1 we denote case C in [13] for upward flow as case A and the new simulation for downward flow as case B. For both cases the length of the unit cell of the Taylor flow (which consists of one bubble and one liquid slug) is $L_{\mathrm{UC}} = 3.5\,\mathrm{mm}$, the gas volume fraction in the unit cells is $\varepsilon_{\mathrm{G}} = 33.1\%$ and the grid consists of 48 × 84 × 48 cubic mesh cells.

3.1. *Influence of flow orientation on* U_{B} / J

By correlating all their experimental data in both circular and square capillaries, Liu et al. [14] proposed for bubble train flow the relation

$$\psi = \frac{U_{\mathrm{B}}}{J} = \frac{1}{1 - 0.61 Ca_{\mathrm{J}}^{0.33}} \tag{26}$$

which is valid for $2\times10^{-4} < Ca_{\mathrm{J}} = \mu_{\mathrm{L}} J / \sigma < 0.39$. Since $Ca_{\mathrm{J}} = Ca / \psi$ relation (26) is equivalent to

$$Ca \cong 4.472 \frac{(\psi - 1)^3}{\psi^2} \tag{27}$$

which is valid in the range $2.08\times10^{-4} < Ca < 0.706$. In Fig. 5 we compare the numerical results for $\psi = U_{\mathrm{B}} / J$ for cases 1 and 2 with Eq. (27) and with experimental data for co-current upward Taylor flow of silicon oil in a square mini-channel with 2 mm × 2 mm cross section [15]. While the numerical results for ψ agree well with these experimental data, they are somewhat higher than predicted by Eq. (27). The numerical data in Fig. 5 show that ψ is larger for upward flow than for downward flow for the same value of Ca. This observation can be explained by the two volumetric forces which drive the flow, namely pressure gradient and buoyancy. While the force due to the pressure gradient acts on both phases, the buoyancy force acts on the gas phase only. In upward flow, where both forces act in the same direction, the net driving force experienced by the gas bubble is larger than that experienced by the liquid. In downward flow, however, pressure gradient and buoyancy act in opposite direction. Thus, the magnitude of the total driving force experienced by the

gas bubble is smaller than the one experienced by the liquid. For this reason U_B / J is, for a given value of U_B or J, larger in upward than in downward flow, so that $\psi_{up} > \psi_{down}$. This has direct implications for the recirculation time. For a circular channel it follows from Eq. (8) that $\tau_{up} > \tau_{down}$. The same holds by virtue of Eq. (22) for rectangular channels.

3.2. Evaluation of recirculation time from DNS data

In the theoretical analysis of section 2 we determined the recirculation time under the assumption that the liquid slug is long enough so that the laminar velocity profile is fully developed. In this section we evaluate τ from direct numerical simulation results. Fig. 6 shows the curves Z_λ from Eq. (17) for $\lambda = \lambda_1$ and $\lambda = 0$ for different values of ψ. For $\lambda = 0$ the curves are close to circular for $\psi > 1.5$. As listed in Table 1, the ratio L_S / D_h is less than 1 for case A and B so that the liquid slug is too short to form a fully developed Poiseuille profile. The evaluation of the axial velocity profile in the middle of the liquid slugs, however, shows that the area A_0 is close to circular also in the DNS. We thus assume that the velocity profile is axis-symmetric and fit it by a third order polynomial in r. Then, the recirculation time can be evaluated from Eq. (7). The results for case A and B are listed in Table 1 and are compared with the theoretical results of Eq. (22), where the values of ψ given in Table 1 are used. The comparison shows that the numerical values of τ are about 68 – 128% higher than the theoretical ones. We attribute these large deviations to the assumptions made for evaluation of τ from the DNS results and to the rather short length of the liquid slug in case A and B.

In Fig. 7 we show the values of τ evaluated from the direct numerical simulations as function of the capillary number. We compare our results with experimental data for a square channel ($D_h = 2\,\text{mm}$) with co-current upward flow [5] and co-current upward and co-current downward flow [6]. Fig. 7 shows that for upward flow the present DNS data for τ agree well with the experimental data in [5] and [6]. For downward flow, all our numerical data lie below the curve representing the experimental data of [5] for upward flow. This confirms the finding of our theoretical study in section 2 that the recirculation time in downward flow is smaller than in upward flow. It is interesting

to note that in contrast Tsoligkas et al. [6] found almost three to four times higher values of τ for downward than for upward flow, see also [16]. Their data for downward flow, obtained at much smaller values of Ca than in our study, are lying above the curve given in [5] for upward flow. From our theoretical analysis in section 2 we conclude that the data for τ in [6] and [16] for downward flow might be erroneous.

3.3. Direct numerical simulations of mass transfer

In this section we investigate the influence of the recirculation time on the wall-to-slug mass transfer in co-current upward and downward Taylor flow numerically. We use the numerical method described in [13] and consider the mass transfer of a dilute species that is without feedback on the hydrodynamics. As initial conditions for the hydrodynamics we use the fully developed flow field for upward and downward Taylor flow of case A and B in Table 1, respectively. For both cases the values of U_{B} and J are constant in time and the bubble shape is steady. The initial conditions for the mass transfer simulations are as follows. In a layer consisting of the four mesh cells closest to the channel walls we set the species concentration to $c_{\mathrm{ref}} = 1\mathrm{mol/m}^3$, whereas it is zero in all other mesh cells. The value of the (non-dimensional) Henry number is set to 100, so that at equilibrium the species concentration in the liquid is 100 times higher than in the gas phase. By this choice we ensure that most of the species stays within the liquid phase. In practice, the species diffusivity in the liquid is typically three orders of magnitude lower than in the gas. Here, we use a species diffusivity of 2×10^{-6} m^2/s - a value which is typical for a gas - for both phases. By this we avoid the necessity to use a very fine grid to resolve the otherwise very thin concentration boundary layer on the liquid side of the interface. Such a simulation would require a huge amount of CPU time which cannot be afforded. The Schmidt number in the liquid phase is then $Sc_{\mathrm{L}} \equiv \mu_{\mathrm{L}} / (\rho_{\mathrm{L}} D_{\mathrm{L}}) = 25$ while that in the gas phase is $Sc_{\mathrm{G}} \equiv \mu_{\mathrm{G}} / (\rho_{\mathrm{G}} D_{\mathrm{G}}) = 7.8$. Within the transient simulation then the species transport by convection and diffusion from the wall region to the liquid bulk and into the bubble is computed.

To quantify the mass transfer we consider the time evolution of the mean species concentration in

the four mesh cell thick layer close to the walls, normalized by the initial species concentration in this region. In addition, we compute this non-dimensional quantity for that axial part of the unit cell, where the liquid slug is present. In Fig. 8 we compare these curves for upward and downward flow. The vertical bars indicate different characteristic time scales for upward and downward flow. Besides T_S and T_L already defined these are $T_B \equiv L_B / U_B$ and $T_{UC} \equiv L_{UC} / U_B$. Fig. 8 reveals that for $t < T_S$ the mass transfer in the liquid slug region is slightly more efficient for downward than for upward flow. As the mean concentration in the center of the liquid slug increases, the curves for upward and downward flow show a crossover and an oscillatory behavior. Within the time interval $T_S < t < T_B$ the slug passes that region of the unit cell which corresponds to the initial bubble position. For this period the slope of the curves in Fig. 8 becomes flatter, indicating that the mass transfer in the liquid slug decreases. The reason for this may be that a certain amount of species from this initial liquid film region is already transferred into the bubble. At time $t = T_{UC}$ the bubble has traveled a distance of one unit cell. Fig. 8 shows that T_S, T_B, and T_{UC} are - due to the lower bubble velocity - all larger for downward than for upward flow. Only T_L is smaller for downward than for upward flow.

Fig. 8 shows that the overall mass transfer in the entire wall region of the unit cell is slightly more efficient for upward than for downward flow for $t > T_{S,up} \approx 0.01\text{s}$. The reason for this behavior is not clear yet. It may have its origin in the longer bubble length of the upward flow (see Table 1). This results in a longer liquid film around the bubble, though the minimum thickness of the liquid film is in upward flow slightly smaller than in downward flow (see bubble diameter D_B in Table1). Another reason may be the different size of the recirculation area A_1 in upward and downward flow. This becomes apparent in Fig. 9 a) and b) which show the streamlines in the liquid phase. Fig. 9 c) and d) show the concentration field for upward and downward flow at equivalent time steps. The images indicate that the concentration in the center of the liquid slug is more uniform for upward than for downward flow. For both cases, the concentration is lowest at the bubble rear. In downward flow, however, the concentration at the rear of the bubble is much lower than in upward flow. We feel that

the rather short liquid slug length used in the present study may not be suitable for clarifying the differences in mass transfer in upward and downward Taylor flow. Therefore, further simulations with a much longer liquid slug and a more suitable initial concentration field are required to further uncover the role of the recirculation time for mass transfer in upward and downward Taylor flow.

4. Conclusions

In this study the liquid slug recirculation time (τ) in laminar Taylor flow through a rectangular channel is investigated analytically and numerically. By assuming a fully developed laminar liquid slug a relation $\tau = \tau(\alpha, \psi)$ is derived, where α is the channel aspect ratio and $\psi = U_B / J$ is the ratio of bubble velocity to total superficial velocity. For practical purposes the theoretical result, which involves definite integrals that have to be evaluated numerically, are fitted by an algebraic expression. For given values of α and ψ, Eqs. (24) and (25) can be used to estimate the time needed by the liquid to move from end of the liquid slug to the other. These results will be useful to develop mechanistic models for mass transfer in Taylor flow.

From the theoretical results it appears that τ is larger in upward than in downward Taylor flow for a given value of ψ because of buoyancy. This conjecture is confirmed by direct numerical simulation results. This suggests that recent experimental data [6], [16], where the opposite behavior is found, may be erroneous.

The lower non-dimensional liquid slug recirculation time suggests that Taylor flow operated in downward mode may be more efficient for the mass transfer path from the bubble ends to the liquid slug and the channel walls than upward Taylor flow. This topic is investigated by direct numerical simulations of wall-to-bulk mass transfer in upward and downward Taylor flow in a square channel at similar values of J. The overall mass transfer who also includes the contribution through the lateral liquid film surrounding the bubbles appears, however, to be slightly more efficient for upward than for downward flow, at least for the conditions investigated here. While the reason for this behavior could not be fully clarified, the results nevertheless indicate that the mass transfer in Taylor flow is a complex phenomenon, which depends on a large number of hydrodynamic and physical-

chemical parameters. Thus, for heterogeneously catalyzed gas-liquid reactions in monolith reactors a general statement whether upward or downward Taylor flow is more efficient for mass transfer is not reasonable.

Acknowledgements

This work originates from a stay of the first author as an LPP exchange student at University Karlsruhe and Forschungszentrum Karlsruhe. The supports of the EU LLP program, of the Institute of Science and Technology and of Forschungszentrum Karlsruhe are gratefully acknowledged.

References

[1] S. Roy, T. Bauer, M. Al-Dahhan, P. Lehner and T. Turek, AIChE J. 50 (2004) 2918.

[2] M.T. Kreutzer, F. Kapteijn, J.A. Moulijn and J.J. Heiszwolf, Chem. Eng. Sci. 60 (2005) 5895.

[3] A.N. Tsoligkas, M.J.H. Simmons and J. Wood, Chem. Eng. Sci. 62 (2007) 5397.

[4] R. Guettel, J. Knochen, U. Kunz, M. Kassing and T. Turek, Ind. Eng. Chem. Res. 47 (2008) 6589.

[5] T.C. Thulasidas, M.A. Abraham and R.L. Cerro, Chem. Eng. Sci. 52 (1997) 2947.

[6] A.N. Tsoligkas, M.J.H. Simmons and J. Wood, Chem. Eng. Sci. 62 (2007) 4365.

[7] R.K. Shah and A.L. London, Laminar flow forced convection in ducts, Academic Press, New York, 1978, p. 197.

[8] H.F.P. Purday, An introduction to the Mechanics of Viscous Flow, Dover Publications, New York, 1949, p. 16.

[9] N.M. Natarajan and S.M. Lakshmanan, Ind. J. Technol. 10 (1972) 435.

[10] M.C. Öztaskin, M. Wörner and H.S. Soyhan, Phys. Fluids 21 (2009) 042108.

[11] Ö. Keskin, M. Wörner, H.S. Soyhan, T. Bauer, O. Deutschmann and R. Lange, Viscous co-current downward Taylor flow in a square mini-channel, AIChE J. (accepted for publ.)

[12] M. Wörner, B. Ghidersa and A. Onea, Int. J. Heat Fluid Flow 28 (2007) 83.

[13] A. Onea, M. Wörner and D.G. Cacuci, Chem. Eng. Sci. 64 (2009) 1416.

[14] H. Liu, C.O. Vandu and R. Krishna, Ind. Eng. Chem. Res. 44 (2005) 4884.

[15] T.C. Thulasidas, M.A. Abraham and R.L. Cerro, Chem. Eng. Sci. 50 (1995) 183.

[16] A.N. Tsoligkas, M.J.H. Simmons and J. Wood, The effect of hydrodynamics on reaction rates in capillary reactor, 6th Int. Conf. Multiph. Flow, ICMF 2007, Leipzig, Germany, 9-13 July 2007.

Figures

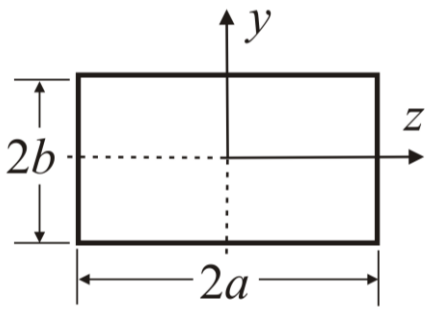

Fig. 1: Sketch of rectangular channel with dimensions and co-ordinate system.

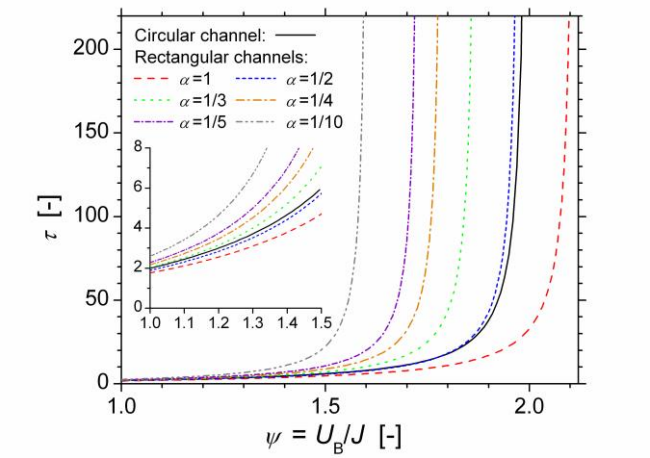

Fig. 2: Recirculation time for circular and rectangular channels as function of ψ and α. The inset graphics is a zoom of the main figure.

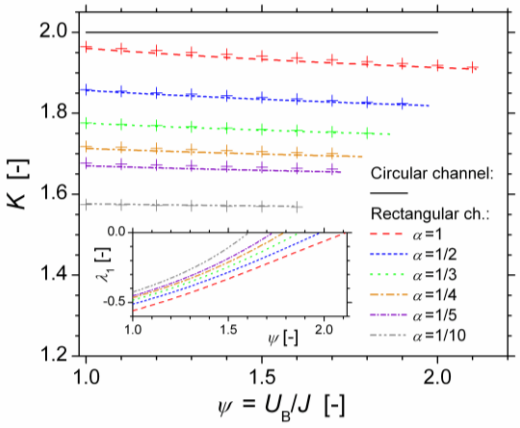

Fig. 3: Dependence of factor K, defined by Eq. (22), on ψ for rectangular channels with different aspect ratio α. The symbols "+" correspond to the fitting by Eq. (24). The inset graphics shows λ_1 over ψ for different values of α.

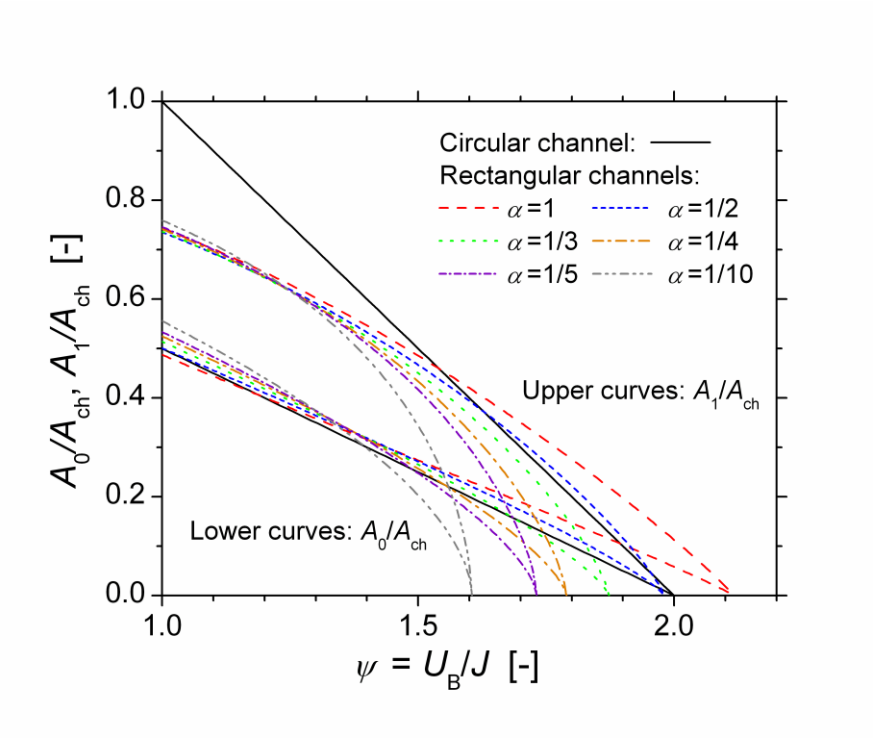

Fig. 4: Non-dimensional area A_1 / A_{ch} and A_0 / A_{ch} as function of ψ for a circular channel and rectangular channels with different aspect ratio α.

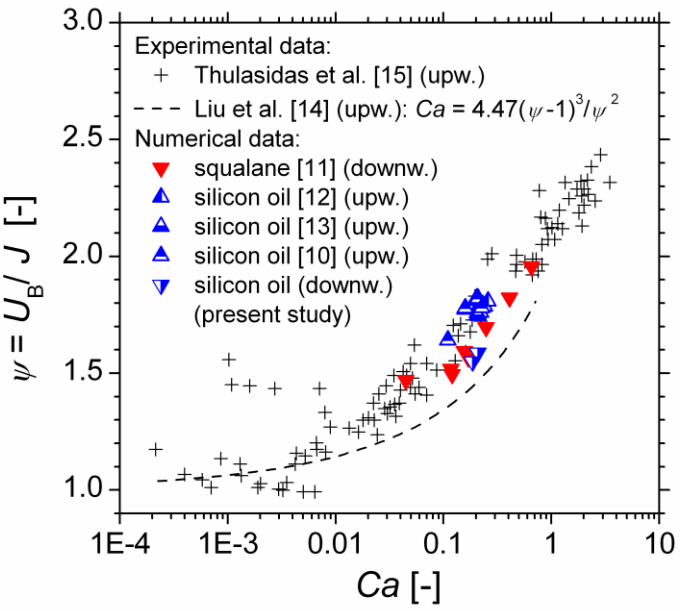

Fig. 5: Velocity ratio ψ as function of capillary number for a square channel. Comparison of DNS results for upward and downward Taylor flow with experimental results for upward flow.

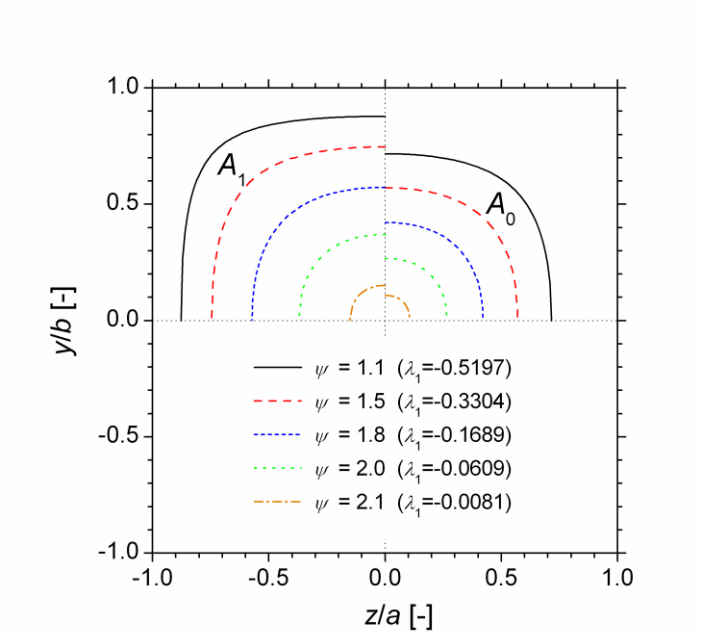

Fig. 6: Cross section of a square channel with shape of area A_1 (upper left quadrant) and A_0 (upper right quadrant) for five different values of ψ. The curves are evaluated from Eq. (17) with $\lambda = \lambda_1$ as given in the figure (for A_1) and $\lambda = 0$ (for A_0), respectively.

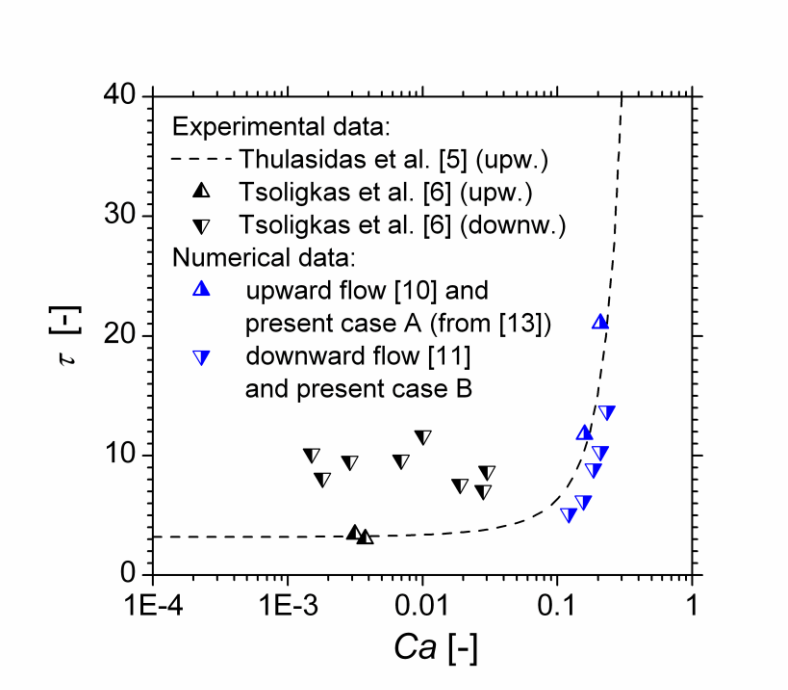

Fig. 7: Recirculation time over capillary number for Taylor flow in a square channel. Comparison of results evaluated from direct numerical simulations with experimental data.

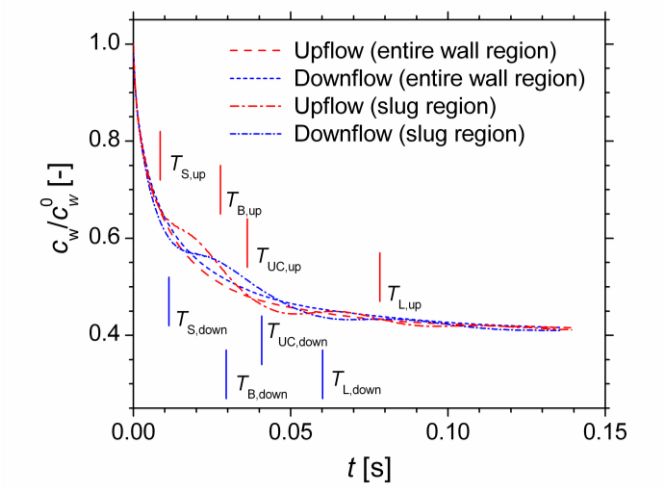

Fig. 8: Time evolution of normalized species concentration in the four mesh cells closest to the channel walls for the liquid slug wall region and the entire wall region. The vertical bars indicate characteristic time scales of the Taylor flow.

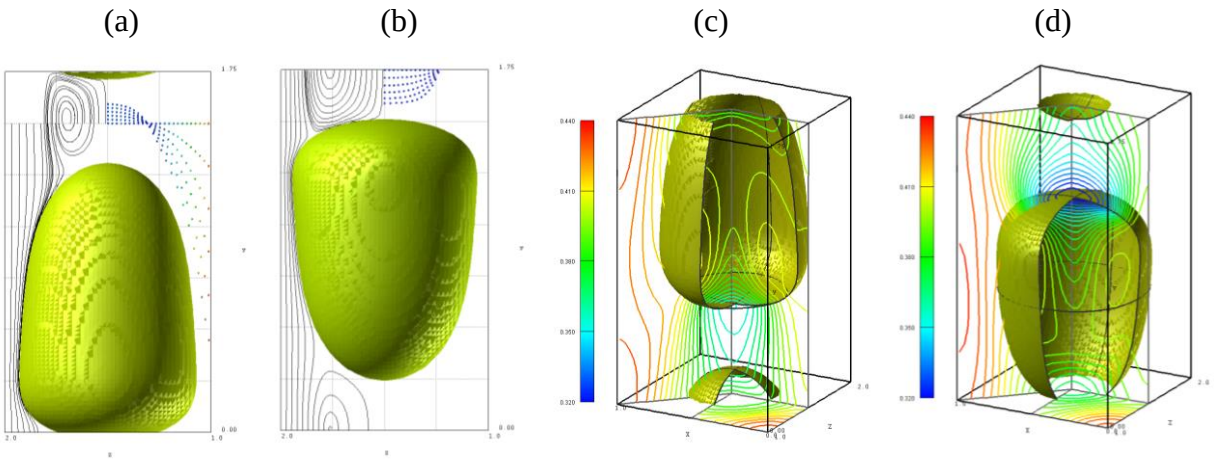

Fig. 9: Visualization of recirculation pattern (left half) and particle trajectories (right half) in liquid slug (a, b) and of concentration $c_L^* = c_L / c_{ref}$ and $c_G^* = Hc_G / c_{ref}$ in different planes for $t = 0.118\,\mathrm{s}$ (c, d) for upward (a, c) and downward flow (b, d).

Tables

Table 1: Simulation results for co-current upward and downward Taylor flow.

Case	Flow direction	J [m/s]	U_B [m/s]	U_L [m/s]	L_S [mm]	L_B [mm]	D_B [mm]	Ca [-]	ψ [-]	τ_{DNS} [-]	τ_{theor} [-]
A	Upward	0.0553	0.0966	0.0349	0.82	2.68	1.72	0.209	1.75	21.1	9.2
B	Downward	0.0552	0.0857	0.0402	0.97	2.53	1.74	0.185	1.55	8.9	5.3